

# Chapter 16

## Non-Destructive Internal Lattice Strain Measurement Using High Energy Synchrotron Radiation

Jun-Sang Park and John Okasinski

**Abstract** High energy synchrotron X-rays can penetrate large samples and real engineering components. Taking advantage of this capability, diffraction techniques using monochromatic X-rays have been widely used to measure the residual strains in engineering components. However, isolating a particular volume inside a large component and measuring the residual strain is a challenge when employing typical monochromatic X-ray techniques. In this work we describe a spiral slit system capable of isolating an interior volume in a polycrystalline sample and non-destructively measuring the lattice strains in the volume. An interference fit sample constructed from a Ni-based superalloy is used to demonstrate the capabilities of the system. We compare the strain results to those measured using a conical slit system, a more mature and established device. The results from several polycrystalline samples with non-cubic crystal symmetry are also presented.

**Keywords** Residual stress • Lattice strain • Synchrotron X-ray • Spiral slits • Conical slits

### 16.1 Introduction

Manufacturing processes can induce residual stress fields in mechanical components. The existence of residual stress in a component is particularly important for predicting the mechanical performance of a component. The ability to characterize the residual stress in a component is, therefore, of significant importance to create components that meet the intended design.

Residual stress characterization techniques can be broadly categorized as destructive and non-destructive. In the non-destructive category, diffraction-based techniques have been quite successful. Neutron scattering based techniques such as the time-of-flight (TOF) method are commonly used to characterize the residual stresses in large components made of high Z materials. With appropriate slitting mechanisms, the residual stresses inside a component can be characterized with spatial resolution on the order of millimeters. Synchrotron X-ray based techniques are also quite popular. The energy dispersive diffraction (EDD) method is sometimes utilized to characterize the residual stresses inside a component. Similar to the TOF method, appropriate slitting mechanisms and stages allow spatial resolution on the order of millimeters longitudinally (along the beam direction) and sub-millimeters perpendicular to the beam.

Residual stress characterization techniques utilizing angle dispersive diffraction (ADD) method is also frequently employed. In this case, the residual stresses can be characterized with micrometer spatial resolution in the direction perpendicular to the beam when appropriate X-ray optics are used. Furthermore, the availability of large area detectors means that many strain components can be measured simultaneously giving the users a more complete picture of the strain. However, in the case of ADD method, the ability to obtain the residual stress information in a volume of material located inside a component is not as simple. In this work, we compare two slitting mechanisms that achieves that task.

### 16.2 Background

Diffraction is governed by Bragg's Law:

$$\lambda = 2d_n \sin \theta_n \quad (16.1)$$

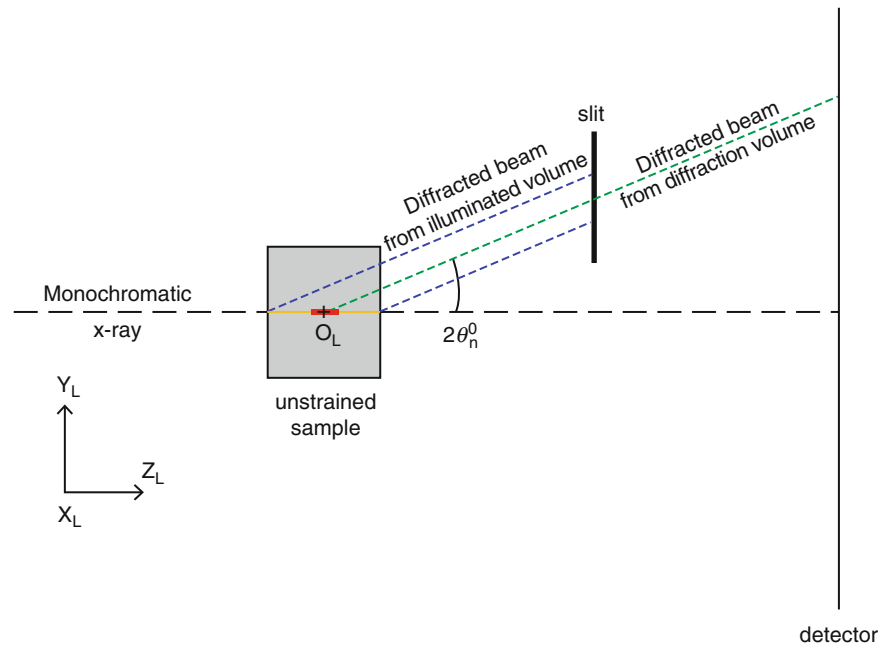
---

J.-S. Park (✉) • J. Okasinski

Advanced Photon Source, Argonne National Laboratory, 9700 S. Cass Avenue, Lemont, IL 60439, USA

e-mail: [parkjs@aps.anl.gov](mailto:parkjs@aps.anl.gov)

**Fig. 16.1** A schematic of slit system to isolate an internal volume for the ADD method. A monochromatic x-ray beam illuminates a volume of material in a sample highlighted in orange. A slit is placed in the path of the diffracted beam emanating from the illuminated volume at a particular angle  $2\theta_n^0$ . Only the diffracted beam from the volume highlighted in red is allowed to pass through the slit and is recorded on the detector



In this equation,  $\lambda$  is the wavelength of the monochromatic X-ray,  $d_n$  is the plane spacing for a family of crystallographic planes  $\{hkl\}$  where its plane normal is denoted by  $\mathbf{n}$ , and  $\theta_n$  is the corresponding Bragg angle.

Several slitting mechanisms for the ADD method to obtain an isolated volume of material located along the X-ray beam have been proposed and demonstrated. For example, Nielsen et al. [1] have proposed a set of conical slits capable of isolating approximately 100–200  $\mu\text{m}$  long volume inside the sample and measured the lattice strains in the volume non-destructively. Martins et al. [2] have proposed a set of spiral slits with similar longitudinal spatial resolution. A set of spider web slits has also been proposed [3].

In all these approaches, the working principle is similar. Figure 16.1 illustrates the geometry associated with the slit mechanism. In this figure, the slit is placed in the path of the diffracted beam. A monochromatic X-ray beam illuminates the entire sample in its path. For a crystalline material, if a slit is placed in the path of the diffracted beam at a reference or unstrained Bragg angle,  $2\theta_n^0$ , with respect to a point in space,  $O_L$ , the diffracted beam from a volume of unstrained material placed at  $O_L$  passes through the slit and is recorded on the detector. It is also the case that if a volume of strained material is placed in the path of the direct beam, the diffracted beam from the material can also pass through the slit and be recorded on the detector as long as the location of the volume is away from  $O_L$ .

In this article, a set of lattice strain measurements from an interference fit sample employing the conical and the spiral slits are presented. The lattice strain results are compared and contrasted. To highlight the advantage of the spiral slits, a set of lattice strain measurement on an interference fit sample manufactured from a titanium alloy is presented.

### 16.3 Experiments

The exact geometries and working principles of the conical slits and the spiral slits used in this work are described in [1] and [2] respectively. Figure 16.2 shows an example diffraction data recorded on the GE amorphous Si area with the conical slits system in place. Figure 16.3 shows an example diffraction data recorded on the area detector with the spiral slit system in place. While the conical slit system captures the full Debye-Scherrer rings with the exception of regions where the four spokes are holding the conical slit system together, only small sections of the Debye-Scherrer rings are recorded when the spiral slits are used.

The geometry of the interference fit sample used in this work is described in detail by Park et al. [4]. Figure 16.4 shows the schematic of the interference fit sample. The sample is composed of a hub manufactured from a nickel superalloy and a shaft manufactured from a tool steel bar stock. The outer diameter of the hub is 24.000 mm and the inner diameters are 12.580 mm and 12.700 mm. The thickness of the hub is 1.250 mm. The diameter of the shaft is 12.7 mm. Because of the tapered inner hole, we anticipate a stress gradient through the thickness of the hub.

**Fig. 16.2** A diffraction image recorded on the area detector with the conical slit system in place. Full Debye-Scherrer rings are recorded on the detector with the exception of the four spokes used to hold the conical slits system intact

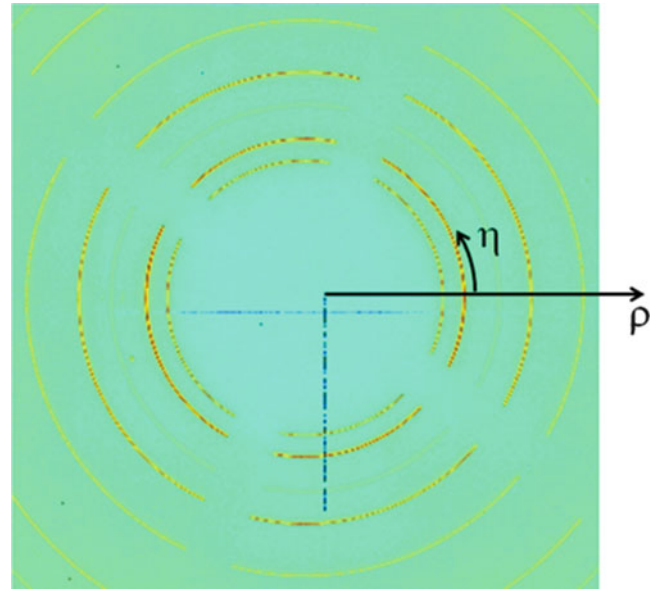
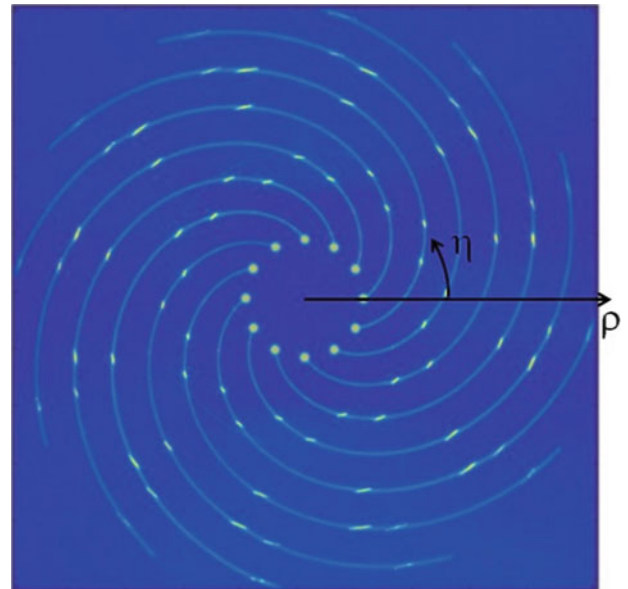


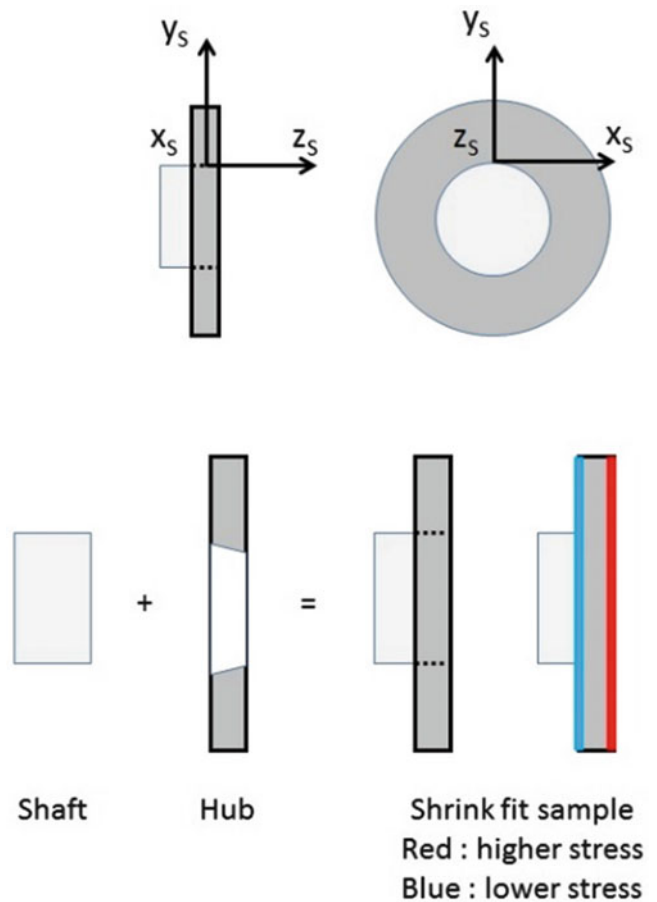
**Fig. 16.3** A diffraction image recorded on the area detector with the spiral slit system in place. There are 12 spiral slits and only partial Debye-Scherrer rings are recorded on the detector



The second interference fit sample manufactured from a titanium alloy is described in Park et al. [5]. In this sample, the inner hole of the hub is not tapered; its inner diameter is 12.636 mm and the outer diameter is 31.750 mm. The thickness of the hub is 1.000 mm. Because there is no taper in the inner hole of the hub, we do not anticipate a stress gradient through the thickness of the hub.

The diffraction data are reduced as described in [2, 6]. To summarize, the detector is calibrated with the  $\text{CeO}_2$  calibration powder data. The diffraction images are binned to produce spectra. The peaks of interest in the spectra are fitted using a pseudo-Voigt function and their peak positions are extracted. In the case of the data set collected using the conical slits, the peak positions as well as the location of the sample with respect to  $O_L$  are used to determine the location of the diffraction volume along  $z$  and the associated strain. In the case of the data set collected using the spiral slits, the radial and the azimuthal positions ( $\rho$  and  $\eta$ ) are used to compute the location of the diffraction volume along  $z$  and the associated strain. In this work, we focus on the nominal  $xx$ - and the  $yy$ - components of strain measured along the  $y$ - $z$  plane on the hub.

**Fig. 16.4** A schematic of the interference fit sample used in this work. The inner hole of the hub is tapered. The hub is heated and a shaft is placed inside the inner hole. When the hub/shaft assembly is allowed to cool, a stress field is imposed on the hub. Larger interference induces larger magnitudes of stresses and smaller interference induces smaller magnitudes of stresses



## 16.4 Results and Discussion

Figure 16.5 shows the  $xx$ - and  $yy$ - components of strain measured along the  $y$ - $z$  plane of the interference fit sample manufactured from nickel superalloy. While there are other reflections available, the  $\{200\}$  reflection was used to measure the strain. As anticipated, the  $xx$ -component of strain is tensile and the  $yy$ -component of strain is compressive in the  $y$ - $z$  plane in both cases. The magnitudes of strain are larger when the interference is larger (at  $z = 0.61$  mm) and are smaller when the interference is smaller (at  $z = -0.61$  mm).

The strains from the conical slits are in general larger in magnitude. This may be attributed to larger azimuthal averaging necessary when the spiral slits are used to measure the strains. When the conical slits are used, the sample is moved along the beam and diffraction images are recorded. Through this motion, the longitudinal strain distribution is measured. Referring to Fig. 16.1, the sample is moved about  $O_L$ . During this motion, the diffracted beams from individual diffraction volumes in the illuminated volume are recorded on the detector. The peak positions from the diffracted beams are used to determine the strains and the location of the diffraction volume inside the hub. As long as the Debye-Scherrer rings show powder-like qualities (no diffraction spots), a small azimuthal bin can be used to integrate the images and to carry out the subsequent analysis. On the other hand, when the spiral slits are used, the location of the peak along a spiral slit is related to the longitudinal location of the diffraction volume; the sample does not have to be translated along  $O_L$ . The consequence of this is that while a great deal of time is saved because the sample is not translated about  $O_L$ , larger azimuthal bins may be necessary.

The real strength of the spiral slits is the ability to deal with non-cubic crystal symmetry. The conical slits used in this work is designed for cubic crystal symmetry. To investigate a polycrystalline material with non-cubic crystal symmetry, one can (1) build a dedicated set of conical slits for the non-cubic crystal symmetry or (2) tune the wavelength of the monochromatic X-ray to allow a small subset of reflections to go through the cubic conical slits. However, both options

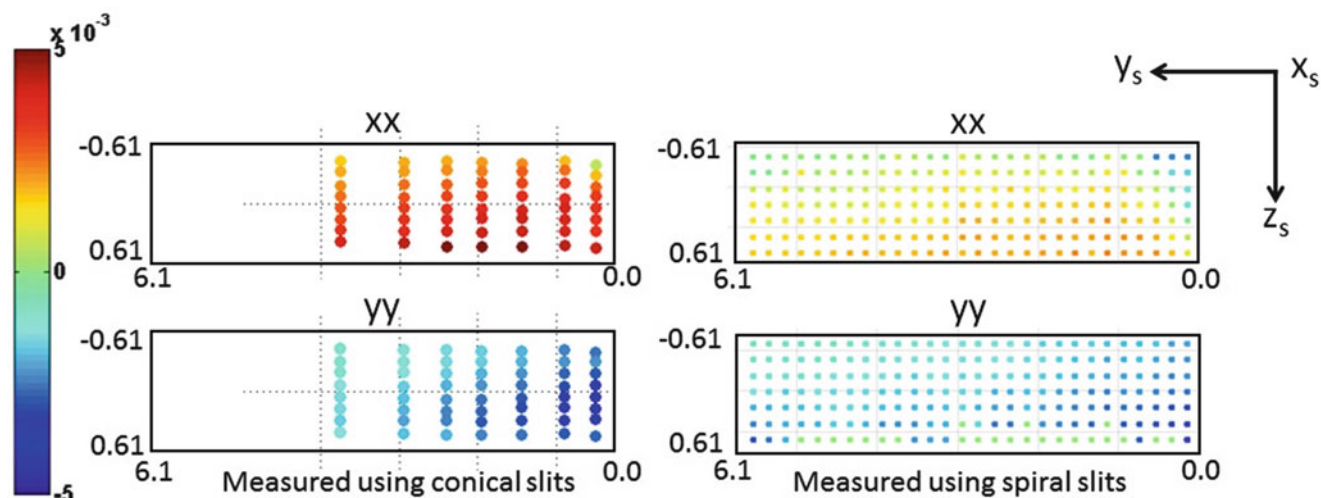


**Fig. 16.5** The  $xx$ - and  $yy$ - components of strain measured along the  $y$ - $z$  plane of the nickel superalloy interference fit sample. The *black boxes* outline the hub dimension in millimeters in the  $y$ - $z$  plane. The locations of the colored dots inside the *black boxes* indicate where measurements were made and the colors of the dots show the magnitude of the strain component. Along  $y$ ,  $y = 0$  mm correspond to the inner most position in the hub and  $y = 6.1$  mm correspond to the outer most position in the hub

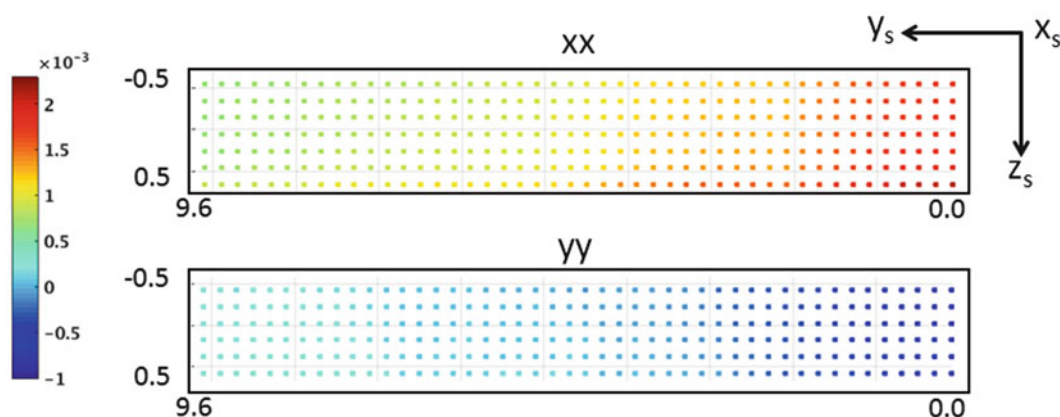


**Fig. 16.6** The  $xx$ - and  $yy$ - components of strain in the hub of the titanium interference fit sample. At  $y = 0.0$  mm, the hub and the shaft are in contact. The strain gradient along the thickness of the hub is measured using the spiral slits

are not optimal. With the spiral slit system, any crystal symmetry can be investigated; with appropriate rotation of either the slit or the sample, the full Debye-Scherrer rings can be measured.

Figure 16.6 shows the  $xx$ - and  $yy$ - components of strain in the hub of the interference fit sample manufactured from the titanium alloy. The  $\{10.2\}$  reflection was used to measure the strains. As anticipated, the  $xx$ -component of strain is tensile and the  $yy$ -component of strain is compressive. The magnitudes of the two components are the largest near the shaft and are the smallest at the outermost position on the hub. There is also a significant strain gradient ( $5 \times 10^{-4}$  difference between the highs and the lows along the thickness of the hub) through the thickness of the hub. This was not anticipated but with the spiral slits, we were able to quantify it.

## 16.5 Conclusions

High energy synchrotron X-rays are capable of penetrating a large structural component to measure the strain in the component. This strain is typically the average strain in the entire volume illuminated by the X-ray in an angle dispersive diffraction setup. With a set of slits placed in the path of the diffracted X-rays, we can also measure the strains in individual

volumes along the beam path. In this work, an interference fit sample manufactured from a nickel superalloy is used to benchmark the conical and the spiral slit systems. We compared the strain fields in an interference fit sample measured using the conical and the spiral slit systems. The measured strains fields compare favorably. We also used an interference fit manufactured from a titanium alloy to demonstrate the spiral slit system's capability to measure the internal strains in a polycrystalline sample with non-cubic crystal symmetry. It is revealed that there is a measurable strain gradient inside the interference fit sample.

**Acknowledgment** The authors appreciate Dr. V. Honkimäki at the European Synchrotron Radiation Facility, France for loaning the spiral slits. This research used resources of the Advanced Photon Source, a U.S. Department of Energy (DOE) Office of Science User Facility operated for the DOE Office of Science by Argonne National Laboratory under Contract No. DE-AC02-06CH11357.

## References

1. Nielsen, S., Wolf, A., Poulsen, H., Ohler, M., Lienert, U., Owen, R.: A conical slit for three-dimensional XRD mapping. *J. Synchrotron Rad.* **7**, 103–109 (2000)
2. Martins, R., Honkimaki, V.: Depth resolved investigation of friction stir welds made from AA2024 / AA2024 and AA2024 / AA6082 using a spiral slit and high energy synchrotron radiation. *Mater. Sci. Forum* **490–491**, 424–429 (2005)
3. Sinsheimer, B. Bouet, S. Ghose, E. Dooryhee and R. Conley.: X-ray powder diffraction with spiderweb slits (poster), 2014
4. Park, J.-S., Lienert, U., Dawson, P.R., Miller, M.P.: Quantifying three-dimensional residual stress distributions using spatially-resolved diffraction measurements and finite element based data reduction. *Exp. Mech.* **53**(9), 1491–1507 (2013)
5. Park, J.-S., Ray, A., Dawson, P., Lienert, U., Miller, M.: Determination of residual stress in a microtextured alpha titanium using high energy synchrotron x-ray. *Journal of Strain Analysis for Engineering Design*, no. accepted
6. Miller, M.P., Bernier, J.V., Park, J.-S., Kazimirov, A.: Experimental measurement of lattice strain pole figures using synchrotron x rays. *Rev. Sci. Instrum.* **76**(11), 113903–113911 (2005)